Journal of Nuclear Materials 92 (1980) 121–135

A NUMERICAL SOLUTION TO THE FOKKER–PLANCK EQUATION DESCRIBING THE EVOLUTION OF THE INTERSTITIAL LOOP MICROSTRUCTURE DURING IRRADIATION

N.M. GHONIEM and S. SHARAFAT
School of Engineering and Applied Science, University of California, Los Angeles, California 90024, USA

Received 24 October 1979

A new calculational method has been developed for the numerical solution of the Fokker–Planck equation describing voids and interstitial loops. Small-size interstitial clusters were studied using a detailed rate theory approach, while large-size loops were simulated by descretizing a transformed Fokker–Planck equation. Interstitial loops containing up to millions of atoms were investigated using this hybrid technique. The numerical results of the model compare reasonably well with previous detailed rate theory calculations, as well as with experimental findings on heavy ion irradiated 316 stainless steel.

1. Introduction

The problem of point defect cluster nucleation and growth in metals under irradiation has been the subject of recent active research [1–14]. Apart from the interesting academic nature of this area, the question of how the microstructure develops during irradiation is of significant technological importance. Irradiation induced swelling, creep deformation, growth, embrittlement, hardening and loss of ductility are all strongly influenced by the nucleation and growth of point defect clusters.

About a decade ago, Brown, Kelly and Mayer [1] carried out calculations for interstitial clustering in graphite. They considered heterogeneous nucleation when one unbound interstitial encounters another interstitial atom bound already to a trapping site such as boron impurities. Recently, Kiritani [2] used a model similar to Brown et al. to explain HVEM experimental results on interstitial loop formation. Vacancy mobility and the existence of divacancies have been included in his analysis.

Hayns [3] studied the nucleation and early stages of growth of interstitial dislocation loops in irradiated materials. A hierarchy of rate equations was solved to simulate the homogeneous nucleation of interstitial dislocation loops. The assumption that diinterstitial atom pairs are stable against thermal dissociation was examined and it was concluded to be appropriate. Lam [4] developed a time and space dependent model to study the radiation induced defect buildup and radiation-enhanced diffusion in a foil under irradiation. The distribution of interstitials, monovacancies and vacancy aggregates containing two to six vacancies in a silver foil under irradiation was calculated as a function of both distance from the surface of the foil and irradiation time by numerically solving the rate equations for various temperatures and internal sink concentrations. In an investigation of interstitial cluster nucleation at the onset of irradiation, Johnson [5] developed rate equations for the concentrations of single and small clusters of vacancies and interstitials. The effects of irradiation temperature and displacement rate were investigated, and it was found that the cluster concentrations are sensitive to cluster binding energies. Hall and Potter [6] included interstitial-impurity trapping in a time-dependent nucleation and growth model that is used to calculate both vacancy and interstitial cluster densities and size distributions during irradiation. Recently, Ghoniem and Cho [7] developed a rate theory model for the simultaneous clustering of point defects during irradiation. Size-dependent bias factors and self-consistent reaction rate constants were used to evaluate the feed-back effects between the vacancy cluster and interstitial loop populations. An atom

conservation principle was used to determine the number of necessary rate equations as a function of irradiation time.

The basic limitation to the rate-theory approach (or equivalently the Master Equation formulation) lies in the one-to-one relationship between the number of simultaneous differential equations and the number of species in a cluster. Although the previously mentioned methods have been detailed enough to analyze fundamental point defect kinetics and to describe the effects of various irradiation and material parameters, the computations become prohibitively expensive for large-size defect clusters.

The need for the correspondence of theory and experiment has prompted the development of approximate computational methods for the kinetics of defect clustering. Kiritani [8] has developed a scheme for the nucleation and growth of clusters in which clusters within a range of sizes are grouped together, and has applied the method to vacancy agglomeration after quenching. Hayns [9] has applied the Kiritani grouping scheme to study the nucleation and growth of interstitial loops during irradiation, and has shown that objections to the method by Koiwa [10] can be surmounted. Hayns [11] also reported calculations using the grouping to study nucleation and growth of interstitial loops under fast-reactor and simulation conditions.

A different approach for studying the nucleation and growth of defect clusters has considered solving continuum equations rather than rate equations. Sprague et al. [12] were able to describe vacancy clusters containing up to 3920 vacancies by descretizing a diffusion-type equation with variable diffusivity. Recently, Wolfer et al. [13] followed similar lines to demonstrate that the rate equations describing the clustering kinetics can be condensed into one Fokker–Planck continuum equation. The latter was interpreted as a diffusion equation with drift terms. They showed that void nucleation and growth can be both incorporated into such a unified formalism. Hall [14] investigated point defect agglomeration considering a different form of the continuum description. Only the cluster concentrations were expanded in a Taylor series and the resulting set of rate equations were shown to be condensed into one partial differential equation.

The majority of the approaches mentioned above have not been able to accurately describe the long term behavior of defect aggregates, either due to the high computational penalties in rate theory methods, or because of the restrictive approximations in grouping methods. Koiwa [10] has developed an analytical solution for the vacancy clustering problem in a special case, and compared it to the results of the grouping method. It was concluded in his study that the approximations in the grouping technique resulted in cluster distributions that deviate from the exact analytical results due to the sensitivity of the method to the group width.

The objective of this work is to develop and apply a new hybrid approach to the problem of point defect clustering. The theoretical predictions are also compared to long term ion simulation experiments. In the next section, we describe the theory and physical model. The numerical analysis and computational aspects are outlined in section 3. Section 4 compares the results of the numerical analysis of the continuum equation to the detailed rate theory solution. High dose irradiation results are presented in section 5 for fusion reactor conditions, and section 6 is concerned with comparing the calculational results to ion simulation data. Conclusions finally follow in section 7.

2. Theoretical model

In developing the theoretical model, we will follow the rate theory formulation of Ghoniem and Cho [7] for small point defect clusters. Separate rate equations will be constructed for single vacancies, single interstitials and clusters of up to 4 vacancies and 4 interstitials. Larger size defects, however, will be simulated by condensing the set of rate equations into one generalized Fokker–Planck equation for both voids and interstitial loops. An outline of this hybrid approach is given below.

2.1. Rate equations

Defect behavior during irradiation has been successfully studied using the rate theory of chemical kinetics in which a set of ordinary differential equations was used to describe the concentration rate of change for various defect species [3–5,7]. The under-

lying principle is to represent the production and removal rates of a particular defect size in a species balance equation. For the sake of self-consistency, we will briefly present the rate theory of Ghoniem and Cho [7], and write the rate equations governing the rate of change of the fractional defect concentrations. The concentrations of single vacancies and vacancy clusters up to tetra-vacancies are governed by

$$\frac{dC_v}{dt} = P + K_i^c(2)\, C_i C_{2v} + (2\gamma_v^c(2) - K_v^c(2)\, C_v)\, C_{2v} + \sum_{x=3}^{x_{max}} (\gamma_v^c(x) - K_v^c(x)\, C_v)\, C_{xv} - \sum_{x=3}^{x_{max}} K_v^1(x)\, C_v C_{xi} + Z_v \rho_d D_v (C_v^e - C_v) - \alpha C_v C_i - K_v^c(1)\, C_v^2 - K_v^1(2)\, C_v C_{2i}\,, \quad (1)$$

$$\frac{dC_{2v}}{dt} = \tfrac{1}{2} K_v^c(1)\, C_v^2 + \gamma_v^c(3)\, C_{3v} + K_i^c(3)\, C_i C_{3v} + \rho_d D_{2v} C_{2v}^e - K_v^c(2)\, C_v C_{2v} - K_i^c(2)\, C_i C_{2v} - \gamma_v^c(2)\, C_{2v} - \rho_d D_{2v} C_{2v}\,, \quad (2)$$

$$\frac{dC_c(x)}{dt} = K_v^c(x-1)\, C_v C_c(x-1) - \{K_i^c(x)\, C_i + K_v^c(x)\, C_v + \gamma_v^c(x)\}\, C_c(x) + \{K_i^c(x+1)\, C_i + \gamma_v^c(x+1)\}\, C_c(x+1)\,, \quad x = 3, 4\,. \quad (3)$$

On the other hand, the equations representing single interstitials and interstitial clusters up to tetra-interstitials are given by

$$\frac{dC_i}{dt} = P + K_v^1(2)\, C_v C_{2i} - K_i^1(1)\, C_i^2 - \alpha C_v C_i - K_i^1(2)\, C_i C_{2i} - K_i^c(2)\, C_i C_{2v} - \sum_{x=3}^{x_{max}} K_i^1(x)\, C_i C_{xi} - \sum_{x=3}^{x_{max}} K_v^c(x)\, C_i C_{xv} - Z_i \rho_d D_i C_i\,, \quad (4)$$

$$\frac{dC_{2i}}{dt} = \tfrac{1}{2} K_i^1(2)\, C_i^2 + K_v^1(3)\, C_v C_{3i} - K_i^1(2)\, C_i C_{2i} - K_v^1(2)\, C_v C_{2i}\,, \quad (5)$$

$$\frac{dC_1(x)}{dt} = K_i^1(x-1)\, C_i C_1(x-1) + \gamma_v^1(x-1)\, C_1(x-1) - \{K_i^1(x)\, C_i + K_v^1(x)\, C_v + \gamma_v^1(x)\}\, C_1(x) + K_v^1(x+1)\, C_v C_1(x+1)\,, \quad x = 3, 4\,, \quad (6)$$

with the following definitions: P = irradiation production rate of Frenkel pairs (at/at/s), α = point defect recombination coefficient (s^{-1}) = $48\nu_i \exp(-E_M^i/kT)$, $K_{i,v}^{1,c}$ = rate constant for i/v impingement on loops/cavities (s^{-1}), ρ_d = straight dislocation density (m^{-2}), $D_{v,i}$ = point defect diffusion coefficients (m^{-2}), D_{2v} = divacancy diffusion coefficient (m^{-2}) = $\nu_v a^2 \exp\{-E_{2v}^m/kT\}$ [15], and C_{2v}^e = divacancy thermal concentration

$$(\text{at/at/s}) = 6 \exp\{-(2E_F^v - E_B^{2v})/kT\}\ [15]\,. \quad (7)$$

Notice that divacancies were assumed to be mobile, and that their major interaction is with dislocations. The definitions of the parameters in the equations and their numerical values are given in table 1. The set of balance eqs. (1)–(7) can be easily derived by considering all possible production and removal rate processes for a particular cluster size. The reader is referred to ref. [16] for a detailed description of the derivation. Only 4 single rate equations for interstitial clusters and 4 similar equations for vacancies are used in this work. Larger size interstitial loops and cavities are characterized using Fokker–Planck continuum equations as will be outlined in the next section. Previous numerical results [7] indicated that the cluster behavior for the first few sizes is highly sensitive to defect parameters and rate constants. Therefore, a detailed analysis is found necessary for clusters up to the tetra-size.

2.2. Continuum description of large sizes

For the purpose of simplifying the analysis, we will introduce the following notations:

$\kappa_1(x) = \gamma_v^1(x) + \beta_i^1(x)$ = growth rate of an interstitial cluster by either vacancy emission ($\gamma_v^1(x)$) or interstitial impingement ($\beta_i^1(x)$),

$\kappa_c(x) = \beta_v^c(x)$ = growth rate of a vacancy cluster by vacancy impingement,

$\lambda_1(x) = \beta_v^1(x)$ = decay rate of an interstitial cluster by vacancy impingement,

$\lambda_c(x) = \gamma_v^c(x) + \beta_i^c(x)$ = decay rate of a vacancy

Table 1
Input parameters for 316 stainless steel

Symbol	Parameter	Numerical value
$\alpha a^2/D_i$	Recombination combinatorial number	48 [20]
$L_i^1(1)$	Interstitial–interstitial combinatorial number	84 [3]
$L_v^c(1)$	Vacancy–vacancy combinatorial number	84 [3]
E_v^m	Migration energy of a single vacancy	2.24×10^{-19} J [21]
E_i^m	Migration energy of a single interstitial	3.2×10^{-20} J [21]
E_v^f	Formation energy of a vacancy	2.56×10^{-19} J [21]
E_i^f	Formation energy of an interstitial	6.54×10^{-19} J [21]
E_{2v}^m	Migration energy of a divacancy cluster	1.44×10^{-19} J [15]
E_{2v}^B	Binding energy of a divacancy cluster	4×10^{-20} J [15]
E_{3v}^B	Binding energy of a trivacancy cluster	1.2×10^{-19} J [22]
a	Lattice parameter	3.63×10^{-10} m [9]
ν_i	Frequency factor for an interstitial	5.0×10^{12} [4]
ν_v	Frequency factor for a vacancy	5.0×10^{13} [4]
Z_v	Vacancy–dislocation bias factor	1.0 [21]
Z_i	Interstitial–dislocation bias factor	1.08 [21]
g	Surface energy	1 J/m^2 [21]

cluster by either vacancy emission or interstitial impingement, where the impingement rates are given by

$$\beta_{v,i}^{c,1} = K_{v,i}^{c,1} C_{1,c} \,. \tag{8}$$

Eq. (3) for a vacancy cluster and eq. (6) for an interstitial cluster of any size "x" can now be lumped into one rate equation

$$\frac{dC_{1,c}(x)}{dt} = \kappa_{1,c}(x-1)\, C_{1,c}(x-1) - [\kappa_{1,c}(x) + \lambda_{1,c}(x)]\, C_{1,c}(x) + \lambda_{1,c}(x+1)\, C_{1,c}(x+1) \,, \quad x > 4 \,. \tag{9}$$

Dropping the cluster subscript (1, c) and expanding the first and last terms of eq. (9) in a Taylor series up to the second term, Wolfer et al. [13] showed that the set of equations (9) can be replaced by one continuum equation of the form

$$\frac{\partial C}{\partial t} = -\frac{\partial}{\partial x}\left\{\mathcal{F}C - \frac{\partial}{\partial x}(\mathcal{D}C)\right\}, \tag{10}$$

where C is a generalized concentration for either type of point defect clusters, and the "drift" function is defined as

$$\mathcal{F}(x,t) = \kappa(x,t) - \lambda(x,t) = \text{point defect net bias flux} \,, \tag{11}$$

and the "diffusion" function by

$$\mathcal{D}(x,t) = \tfrac{1}{2}\{\kappa(x,t) + \lambda(x,t)\} = \text{point defect average diffusion flux} \,. \tag{12}$$

The last equation is used to present both vacancy and interstitial clusters, with the appropriate $\mathcal{F}$ and $\mathcal{D}$ functions, for sizes containing more than four atoms.

Eq. (10) is the well known form of the Fokker–Planck equation that describes diffusion in a drift field [17].

2.3. Log-size transformation

The Fokker–Planck formulation presented by eq. (10) has been the subject of investigation in various areas of physics [17–19], especially the physics of a non-equilibrium system of particles [17]. This equation describes the combined time dependent nucleation and growth regimes of the microstructure. However, even with the simplest initial and boundary conditions, the equation proved to be difficult to solve analytically in its general form [18,19].

In order to realistically define the microstructural behavior after large irradiation doses, we will introduce a new variable that is related to the defect radius by a logarithmic transformation:

$$u = \ln(2r/b)\,, \tag{13}$$

where r is the cluster radius and b is the Burgers vector. Also let us define the following quantities

$$n = 2 \text{ for loops}\,, \quad n = 3 \text{ for voids}\,; \tag{14}$$

$$B_2 = \Omega/\pi b \text{ for loops}\,, \quad B_3 = 3\Omega/4\pi \text{ for voids}\,, \tag{15}$$

where $\Omega \approx b^3$ = atomic volume, x_I = number of interstitials in an interstitial loop, x_c = number of vacancies in a cavity, r_I = interstitial loop radius, and r_c = cavity radius.

The following relationships can then be easily verified:

$$r_c = (3\Omega x_c/4\pi)^{1/3} = (B_3 x_c)^{1/3} = \tfrac{1}{2} b\, e^{u_c}\,, \tag{16}$$

$$r_I = (\Omega x_I/\pi b)^{1/2} = (B_2 x_I)^{1/2} = \tfrac{1}{2} b\, e^{u_I}\,, \tag{17}$$

or generally, for both cavities and loops

$$r = (B_n x)^{1/n} = \tfrac{1}{2} b\, e^{u}\,, \tag{18}$$

and

$$u = \frac{1}{n} \ln\left(\frac{2}{\pi} n x\right)\,. \tag{19}$$

Using

$$\frac{\partial}{\partial x} = \frac{\partial}{\partial u}\frac{\partial u}{\partial x} = \frac{1}{nx}\frac{\partial}{\partial u} = \frac{2}{\pi} e^{-nu}\frac{\partial}{\partial u}\,, \tag{20}$$

the describing eq. (10) would now transform to

$$\frac{\partial C(u,t)}{\partial t} = -\frac{2}{\pi} e^{-nu}\frac{\partial}{\partial u}\left[\mathcal{F}C - \frac{2}{\pi} e^{-nu}\frac{\partial(\mathcal{D}C)}{\partial u}\right],$$

which reduces to

$$\frac{\partial C}{\partial t} = \frac{2}{\pi} e^{-nu} \times \left[\frac{2}{\pi} e^{-nu}\left(\frac{\partial^2(\mathcal{D}C)}{\partial u^2} - n\frac{\partial(\mathcal{D}C)}{\partial u}\right) - \frac{\partial(\mathcal{F}C)}{\partial u}\right]. \tag{21}$$

Eq. (21) is quite general and shows independence of the cluster type, except through $\mathcal{D}$, $\mathcal{F}$ and n.

2.4. Numerical analysis

The approach we use here to solve the transformed equation is strictly numerical. In this regard, we first descretize the independent variable u, and then develop expressions for all the dependent variables only at the discrete points. The first and second derivatives are represented by first order, central finite differences.

The numerical solution is sought only at discrete values of the variable u, that is given by

$$u(k) = (k-4)\,h + u(4)\,, \quad k \geqslant 4\,. \tag{22}$$

The value $u(4)$ corresponds to tetra-clusters;

$$u(4) = \frac{1}{n}\ln\left(\frac{2}{\pi} n \cdot 4\right), \tag{23}$$

which is 0.6821 for cavities and 0.8140 for interstitial loops. In implementing the numerical solution, we replace the derivatives in the variable u by central differences, obtaining:

$$\begin{aligned}\frac{\partial C(k)}{\partial t} = {} & \frac{2}{\pi} e^{-nu(k)} \times \left\{\left[\frac{e^{-nu(k)}}{\pi h}\mathcal{D}(k+1)\left(\frac{2}{h} - n\right)\right.\right. \\ & \left. - \frac{1}{2h}\mathcal{F}(k+1)\right] C(k+1) \\ & - \left[\left(\frac{4\, e^{-nu(k)}}{\pi h^2}\mathcal{D}(k)\right)\right] C(k) \\ & + \left[\frac{e^{-nu(k)}}{\pi h}\mathcal{D}(k-1)\left(\frac{2}{h} + n\right)\right. \\ & \left.\left. + \frac{1}{2h}\mathcal{F}(k-1)\right] C(k-1)\right\}. \end{aligned} \tag{24}$$

Now define the new functions

$$\Psi(k, J) = \left(\frac{2\,e^{-nu(k)}}{\pi h}\right)^2 \mathcal{D}(J)$$

$$= \text{diffusion function}, \tag{25}$$

$$\Phi(k, J) = \frac{2n}{\pi^2 h}\, e^{-2nu(k)} \mathcal{D}(J) + \frac{1}{\pi h}\, e^{-nu(k)} \mathcal{F}(J)$$

$$= \text{diffusion-drift function}. \tag{26}$$

With the new definitions introduced in (25) and (26), the basic equation (24) can now be written in a simpler form as

$$\frac{dC(k)}{dt} = \{\Psi(k, k-1) + \Phi(k, k-1)\}\, C(k-1)$$

$$- 2\Psi(k, k)\, C(k)$$

$$+ \{\Psi(k, k+1) - \Phi(k, k+1)\}\, C(k+1). \tag{27}$$

In matching the continuum and rate theory solutions, the diffusion and diffusion-drift functions given by eqs. (25) and (26) were multiplied by the factors m^2 and m, respectively, for the $(k, k-1)$ values in only the first continuum equation. The numerical factor m was determined as follows:

$$m = \frac{\text{step size}}{u(5 \text{ points defects}) - u(4 \text{ point defects})}$$

$$= \frac{nh}{\ln(5/4)}.$$

This ensures that the reaction rates between the last rate theory equation and the first continuum equation are independent of the step size h.

2.5. Calculations of microstructure parameters

The developments outlined in the previous sections will yield the fractional concentrations of point defect clusters at discrete points at any irradiation time. In comparing with experimental data, however, one would be interested in characterizing parameters such as the total defect density, the average radius of both loops and cavities and the dislocation density for loops or sink strength for cavities. In the present calculations, the development of the void sink and its effects on the interstitial loop microstructure were neglected. Experimental data indicate that the dislocation microstructure develops much faster than the corresponding cavity microstructure [26]. Therefore, we will only develop equations for the dislocation loop microstructure.

The total concentration of interstitial loops per unit volume $N_{\text{tot}}(t)$ is given by:

$$N_{\text{tot}}(t) = \frac{1}{\Omega}\int_0^{\infty} C(x, t)\, dx \approx \frac{1}{\Omega}\sum_{x=2}^{x_{\max}} C(x, t)\, \Delta x,$$

$$\Delta x \geqslant 1. \tag{28}$$

And since,

$$\pi r^2 b = x b^3 \tag{29}$$

or

$$\Delta x \simeq (2\pi r/b^2)\, \Delta r, \tag{30}$$

it is easily concluded from eqs. (28) and (30) that

$$N_{\text{tot}}(t) \simeq \frac{2\pi}{\Omega b^2}\sum_{r_{\min}}^{r_{\max}} C(r, t)\, r\, \Delta r. \tag{31}$$

The average radius of an interstitial loop is given by

$$\overline{R_1^s} = \int_0^{\infty} C(x, t)\, r(x)\, dx \Big/ \int_0^{\infty} C(x, t)\, dx \tag{32}$$

or approximately

$$\overline{R_1^s} \simeq \sum_{r_{\min}}^{r_{\max}} C(r, t)\, r^2\, \Delta r \Big/ \sum_{r_{\min}}^{r_{\max}} C(r, t)\, r\, \Delta r. \tag{33}$$

On the other hand, the radius of the loop of an average area is obtained as follows:

$$\text{Average area} = \pi[\overline{R_1^a}]^2 = \bar{x} b^2 \tag{34}$$

or

$$\overline{R_1^a} = \left(\frac{b^2}{\pi}\bar{x}\right)^{1/2}, \tag{35}$$

where

$$\bar{x} = \sum_{i=2}^{i=I_{\max}} x_i C_i\, \Delta x_i \Big/ \sum_{i=2}^{i=I_{\max}} C_i\, \Delta x_i. \tag{36}$$

Using the relations in eqs. (29) and (30), we obtain

$$\overline{R_1^a}(t) = \left[\sum_{r_{min}}^{r_{max}} r_i^3 C_i(r, t)\, \Delta r_i \Big/ \sum_{r_{min}}^{r_{max}} r_i C_i(r, t)\, \Delta r_i \right]^{1/2} . \tag{37}$$

If we now define M_j as the jth moment of the fractional radial distribution, i.e.

$$M_j = \sum_{r_{min}}^{r_{max}} C_i(r, t)\, r_i^j\, \Delta r_j , \tag{38}$$

the following quantities can be easily calculated:

$$N_{tot} = (2\pi/\Omega b^2) M_1 , \tag{39}$$

$$\overline{R_1^s} = M_2/M_1 , \tag{40}$$

$$\overline{R_1^a} = (M_3/M_1)^{1/2} , \tag{41}$$

$$\rho_{loop} = (2\pi/b)^2\, \Omega^{-1} M_2 \tag{42}$$

Eq. (39)–(42) represent average quantities that are calculated as functions of irradiation time.

In the present calculations, the loss terms of point defects to the developing microstructure have been approximated using eqs. (47)–(50). Also, the cavity sink was found to be unimportant up to doses of ~1 dpa. Therefore, the summations

$$\sum_{x=3}^{x_{max}} (\gamma_v^c(x) - K_v^c(x)\, C_v)\, C_{vx}$$

in eq. (1), and

$$\sum_{x=3}^{x_{max}} K_v^c(x)\, C_i C_{vx}$$

In eq. (4) were neglected throughout the calculations. On the other hand, we used the following substitutions:

$$\sum_{x=3}^{x_{max}} K_v^1(x)\, C_v C_{xi} \triangleq Z_v D_v \left(\frac{2\pi}{b}\right)^2 \Omega^{-1} M_2 C_v , \tag{43}$$

$$\sum_{x=3}^{x_{max}} K_i^1(x)\, C_i C_{xi} \triangleq Z_i D_i \left(\frac{2\pi}{b}\right)^2 \Omega^{-1} M_2 C_i . \tag{44}$$

The reaction rate constants $K_{v,i}^{c,1}(x)$ and the vacancy emission rates $\gamma_v^{1,c}(x)$ were calculated using the size dependent bias factors estimated by Wolfer [23]. It is also assumed that point defect interaction with clusters is governed by a combination of bulk diffusion and surface reaction kinetics. This is discussed in ref. [16], where the reaction rates are calculated by analyzing point defect transport along lines similar to the heat transfer in different media.

3. Computational aspects

The set of single rate equations (1)–(6) and the descretized Fokker–Planck equations (35) are solved using the GEAR package [24], which is designed for stiff non-linear ordinary differential equations.

The computational requirements of the present approach are modest when compared to more extensive rate theory calculations. For example, 600 CPU seconds were required to study the interstitial loop microstructure development up to a total dose of 10 dpa. In this typical computer run we used a maximum of 21 equations to simulate the irradiation conditions of 316 stainless steel irradiated at 600°C and a dose rate of 10^{-3} dpa/s. An initial dislocation density of 10^{13} m/m^3 was chosen, and the material parameters of table 1 were adopted in the calculations. The number of continuum rate equations was dynamically increased by bounding the ratio of the largest cluster size concentration to the peak size concentrations with an error criterion ($\epsilon \leqslant 10^{-2}$). This is a less accurate version of the more general conservation principle discussed in ref. [7].

4. Comparison with detailed rate theory calculations

In an earlier study of point defect clustering kinetics [7], a detailed time-dependent rate theory was developed to study the early stages of this phenomenon. The ability to describe the microstructure after long irradiation periods was found to be restricted by extensive computational requirements. In this section, we apply the present formulation to simulate the microstructure evolution of stainless steel under reactor conditions, and compare the results of the calculations to the previous rate theory

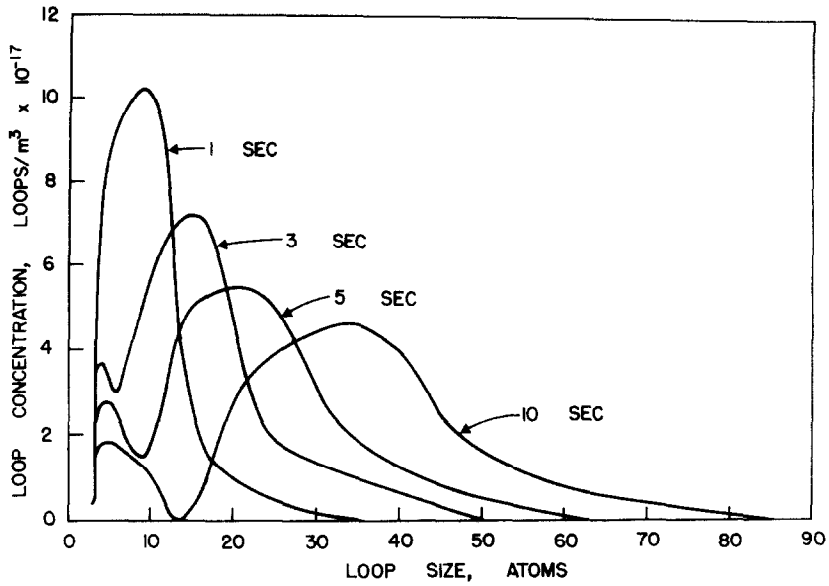

Fig. 1. The development of the loop size distribution for 316 SS. Dose rate = 10^{-6} dpa/s, temperature = 723 K, $\rho_d = 10^{13}$ m/m^3 and $\Delta u_K = 0.203$.

computations. In addition to the parameters of table 1, we use the following: irradiation temperature = 723 K, initial dislocation density = 10^{13} m/m^2, and dose rate = 10^{-6} dpa/s.

Loop size distributions for this reference case are shown in fig. 1 at various irradiation times. Initially, the size distribution is sharp, with most of the interstitial loops containing only few atoms. This is due to the large forward reaction rate for the formation of diinterstitials, which in turn helps to create loops of small size. As irradiation proceeds, more interstitial atoms agglomerate into loops, and consequently the

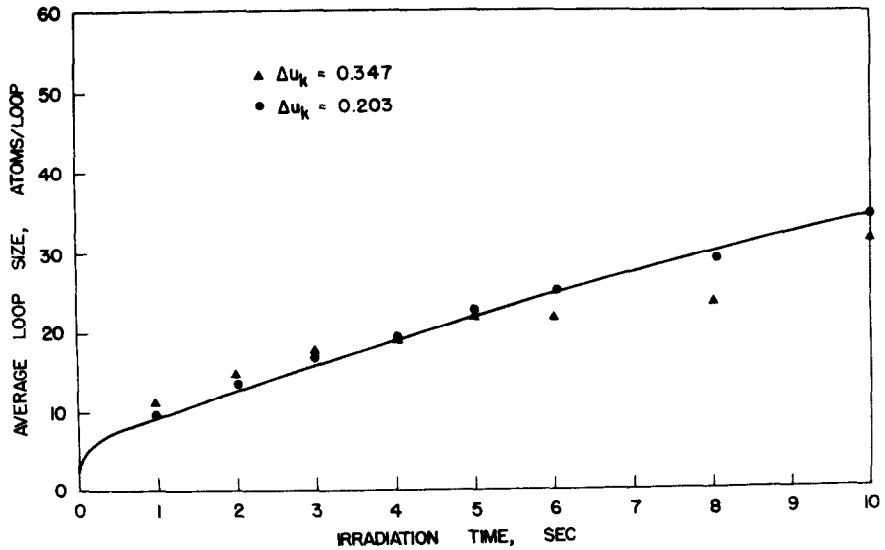

Fig. 2. Average loop size as a function of irradiation time. The solid line represents the full single equation solution, while data points are for the numerical solution.

size distribution broadens. The area under the curve is proportional to the total loop concentration. Notice that a smaller peak of the distribution exists at the tetra-interstitial loop size. This behavior is due to a discontinuity in the reaction rates, where diinterstitials and triinterstitials were treated as spherical clusters, while loops of 4 atoms or larger were considered as atomic disks [16]. The speed at which the distribution moves in cluster size space can be measured in terms of the time behavior of the average size. This is shown in fig. 2, where the average loop size is plotted as a function or irradiation time for small mesh spacing ($\Delta u_k = 0.203$), and for larger mesh spacing ($\Delta u_k = 0.347$). The results are also compared to the complete solution of single rate equations from our previous work [7]. It is interesting to observe that the present numerical results agree within a reasonable error band with the more detailed solution using single rate equations. It can also be seen from the figure that the average size grows almost linearly after an initial transient at the beginning of irradiation.

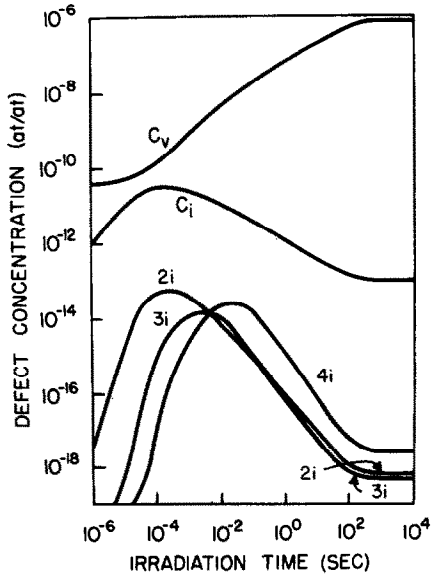

Fig. 3. Time dependence of small-size defect cluster concentrations at 723 K and a dose rate of 10^{-6} dpa/s.

5. Temperature effects on the loop evolution at low dose rates

The wide range of fusion reactor concepts makes it difficult to generalize conclusions of the effects of irradiation on the structural materials used in their designs. However, if we restrict ourselves to studying the microstructure evolution of long burn-cycle fusion machines, such as the tokamaks or mirrors, we should be able to obtain results that are concept-independent. In this section, we study the characteristics of interstitial loop microstructure evolution in representative fusion reactor conditions. For practical considerations, we select to study a 316 stainless steel first wall irradiated at an average low displacement rate of 10^{-6} dpa/s, and the same conditions of the previous example. The microstructural behavior at irradiation temperatures of 773 and 873 K is examined here.

The time-dependence of the small size defect concentrations at 773 K is shown in fig. 3. After about 1 ms, the single vacancy and interstitial behavior is controlled by mutual recombination, and the point defects tend eventually to their steady-state values in ~1000 s. The diinterstitial concentration peaks around 0.1 ms and then declines to a steady-state value. The large peak concentration of diinterstitials acts as a driving force for the nucleation of triinterstitial clusters, which plays a similar role in forming tetrainterstitials. After about 1000 s (~10^{-3} dpa), the concentrations of these clusters achieve approximate steady-state equilibrium values. Although the concentrations of small size clusters reach steady-state equilibrium, the concentrations of larger sizes are found to continue being strongly time-dependent. Fig. 4 shows the time behavior of large-size loop concentrations (containing up to ~1000 interstitials). The interesting feature here is the wide variation of the time constants of different cluster sizes. It can be seen from the figure that is takes a much longer irradiation time for the concentrations of larger size loops to reach steady-state.

The total interstitial loop concentration and the loop line dislocation density as functions of irradiation time at two different temperatures are shown in fig. (5). The important features of this figure is the rapid transients in both of these quantities, which terminate very early during irradiation (~0.1 s). The total loop concentration and the dislocation density increase gradually with irradiation after the initial

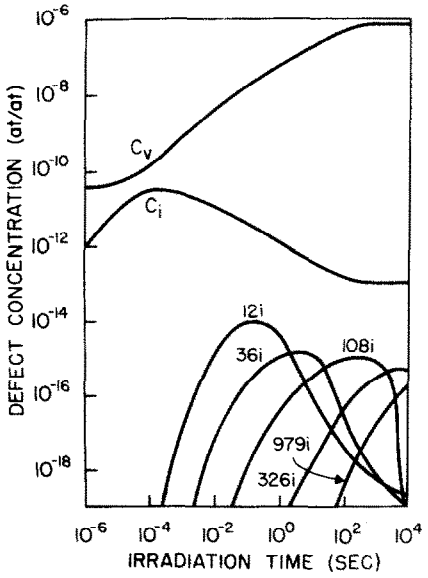

Fig. 4. Large-size interstitial loop concentrations at 773 K and 10^{-6} dpa/s.

transients. Notice that the total accumulated dose is small at the end of the irradiation (10^{-2} dpa), and that the densities are still relatively low. The average loop radius is shown as a function of irradiation time in fig. 6 for both 773 and 873 K. The average radius

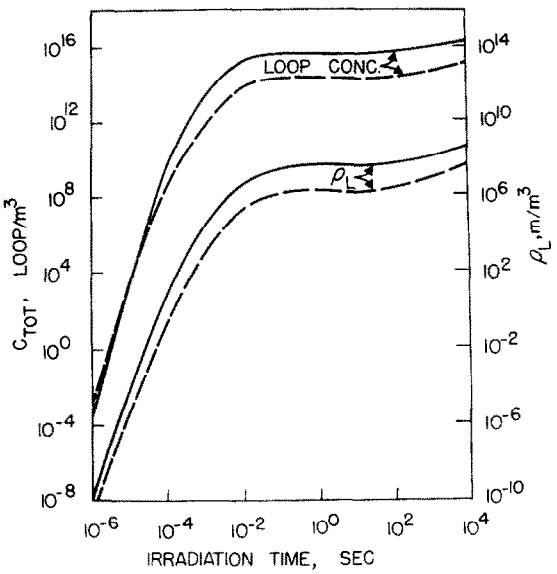

Fig. 5. Temperature effects on the total loop concentration and dislocation density. The solid lines are for 773 K while the dashed are for 873 K.

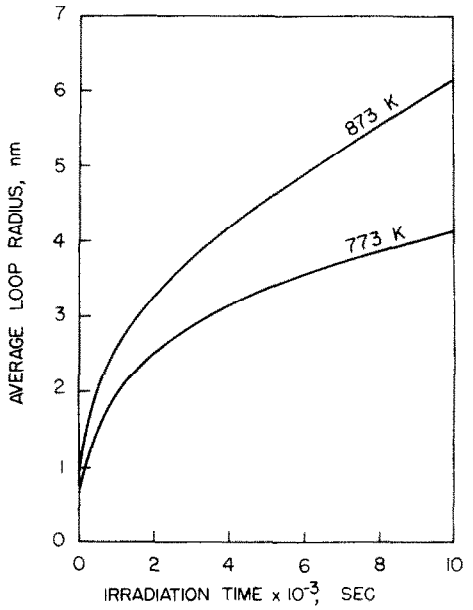

Fig. 6. Average interstitial loop size as a function of irradiation time at 773 and 873 K.

increases rapidly at the start of irradiation, and then shows a slower time dependence as irradiation proceeds.

At the higher temperature of 873 K, the general behavior of the clustering kinetics is similar to that at 773 K. However, the time constants for similar clustering events are much shorter. High temperatures enhance the diffusion controlled point defect clustering kinetics, and the recombination limited regime establishes quasi-steady-state concentrations after only ~100 s at 873 K. Figs. 5 and 6 indicate that the average loop radius is larger while the total dislocation density and loop concentration are both smaller at the higher temperature. This is in line with EBR-II experimental observations [25] at similar dose rates. Fig. 7 shows the temperature effects on the loop size distribution expressed as the fraction of loops in size interval per size interval (for convenience of comparison with experiments). The higher irradiation temperature is observed to cause a shift in the distribution towards larger sizes. This is attributed mainly to the shorter time constants at the high temperature as discussed earlier. In the next section, we compare the results of the calculations using the present model with heavy ion simulation data.

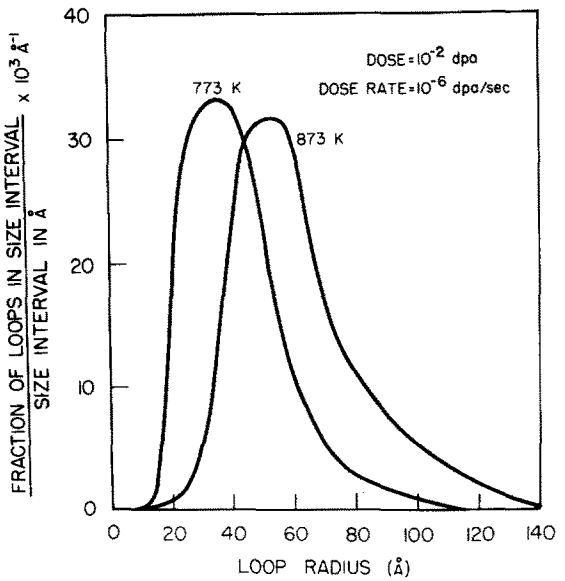

Fig. 7. The temperature effect on the interstitial loop size distribution at low dose rate.

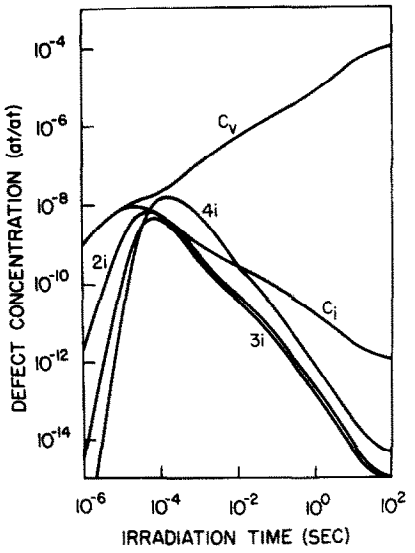

Fig. 8. Time dependent concentrations for small-size defects at 673 K and 10^{-3} dpa/s.

6. Comparison with ion simulation experiments

Recently, Williams [26] performed experiments to study solution-treated type 316 austenitic steel irradiated to low doses in the Harwell Variable Energy Cyclotron. Specimens have been irradiated with 46.5 MeV Ni^{6+} ions and 22 MeV C^{2+} ions, after room temperature pre-injection with 10 ppm helium and without helium pre-injection, at temperatures in the range 300–600°C. In his analysis of the microstructure, the simple arithmetic mean diameter $\bar{d}_{1d}$ was used in the estimation of the dislocation density. The diameter of a loop of mean area, $\bar{d}_{1a}$, where

$$\bar{d}_{1a} = \left(N_{tot}^{-1} \sum_{i=1}^{N} d_i^2 \right)^{1/2}$$

was used in the estimation of the number of interstitial atoms contained in dislocation loops.

The loops were found to be uniformly distributed throughout irradiated areas that were free of grown-in dislocations prior to irradiation. Our assumptions of homogeneous (space independent) reaction rates seem to be reasonable in view of this observation. The loop number density was found to decrease and the mean loop size to increase with increasing irradiation temperature. Loop numbers and sizes appeared not to be significantly affected by the presence of pre-injected helium.

6.1. Low temperature simulations

The time dependencies of single point defects at 673 K are displayed in fig. 8, along those for di-, tri-, and tetra-interstitial clusters. A displacement rate of 10^{-3} dpa/s and the material input parameters of the previous examples are used in these simulations. The high displacement rate used in the present calculations has the effect of increasing the fractional concentrations of defect clusters. A relatively large concentration of tetra-interstitial clusters (10^{-8} at/at) peaks around 0.1 ms. This contrasts with low dose rate irradiations where the peaking occurs at much longer times (~0.1 s). The rapid development of tetra-interstitial peak concentration due to the high displacement rate promotes interstitial clustering, and loop formation occurs at a much faster rate. Large size loop concentrations were found to increase rapidly, and by ~100 s (0.1 dpa) loops containing ~3000 interstitials maintain a relatively large fractional concentration (10^{-12} at/at).

The average loop radius as a function of irradiation time increases rapidly at the beginning of irradiation

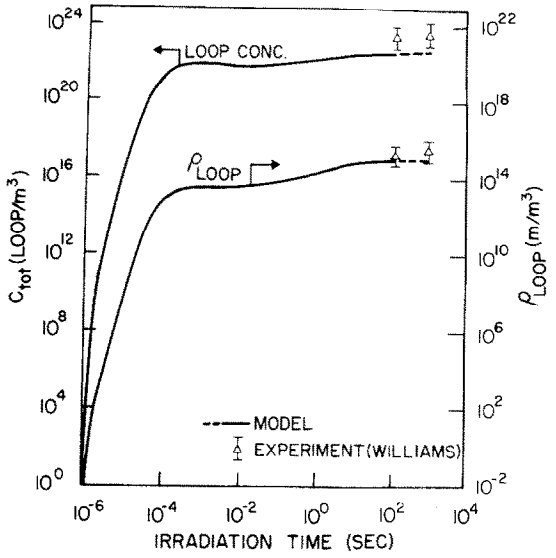

Fig. 9. A comparison of the results of the calculations with experimentally determined loop concentrations and line densities at 673 K and 10^{-3} dpa/s.

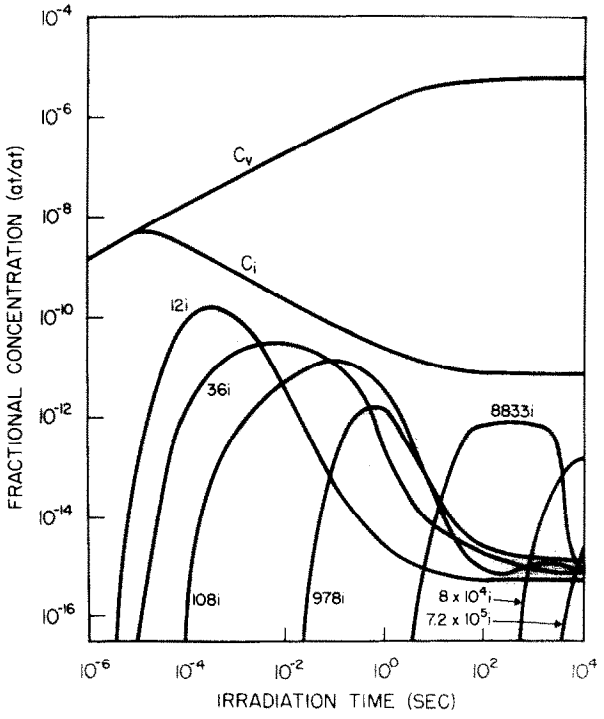

Fig. 10. Time dependence of the clustering process for large-size interstitial loops at 873 K and 10^{-3} dpa/s.

as a result of the enhanced clustering kinetics at this high displacement rate. While the predicted value of the average radius after 100 s is ~55 Å, the experimentally measured radius is reported as 15 Å [26].

Although it is intended to correlate the model results with experimental data, we realize the relative simplicity of the physical picture presented by our formulation. Collision cascade effects in ion bombardment experiments [27], impurity effects in complex alloys such as 316 stainless steel [28] and grown-grown-in dislocation dynamics are just examples of added physics that can be important. For example, a high initial dislocation density has been shown to reduce the average loop size [16]. Fig. 9 compares the results of our calculations to the experimentally measured total loop concentration and dislocation density. The two parameters exhibit rising transients at the start of irradiation establishing values that are close to those measured experimentally, in only about a millisecond. This behavior supports the approximation of a constant loop number density in microstructure growth calculations [27].

6.2. *High temperature simulations*

At high temperatures, point defect diffusion and interaction rates increase, which speeds up the dynamics of clustering. Generally, the higher point defect mobilities result in lower defect concentrations. At high temperatures, it is then expected that point defect agglomeration is fast and results in low concentrations of microstructural features (such as interstitial loops or cavities). The peak concentration of tetra-interstitials at 873 K is actually observed to form very quickly at ~50 μs and to be ~2 orders of magnitude lower than the corresponding value at 673 K.

The clustering processes of large-size interstitial loops are shown in fig. 10, where the fractional concentrations are shown as functions of irradiation time. With the present calculational technique, loops containing up to several million interstitial atoms are simulated. One can easily observe some general trends in the behavior of interstitial agglomeration. The concentration rises to a maximum and then declines to an equilibrium value. The time scales for achieving either a maximum or an equilibrium concentration increase with increasing loop size. It is also noticed that the absolute fractional concentrations go down

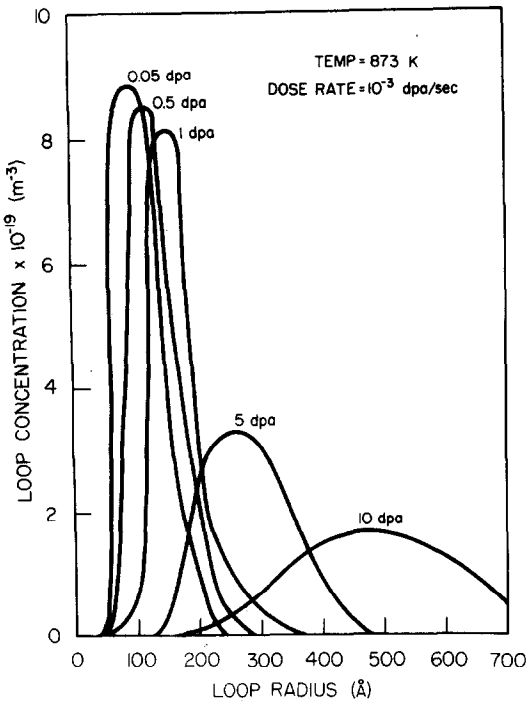

Fig. 11. Evolution of the interstitial loop size distribution at high dose rates.

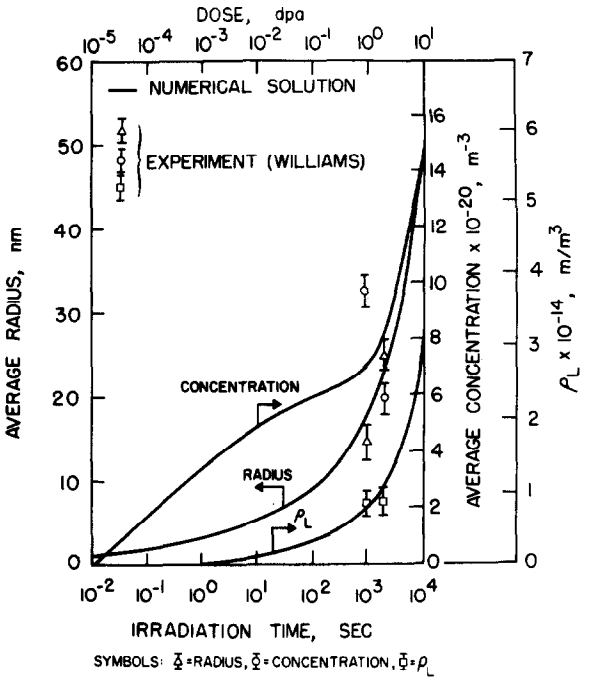

Fig. 12. Comparison between theory and experiment of the interstitial loop parameters at 873 K and 10^{-3} dpa/s.

for large size loops, since each loop contains a very large number of interstitial atoms. The development of the loop size distribution at 873 K is shown in fig. 11. With increasing irradiation dose, the peak of the distribution broadens and also shifts towards larger radii.

The results of the numerical simulations are compared to the experimental data of Williams [25] in fig. 12. We compare the calculations with the data obtained from 1150°C solution-treated type 316 stainless steel specimens irradiated to 1 and 2 dpa with 46.5 MeV Ni^{6+} ions at 600°C with no helium pre-injection. Fig. 12 shows the average radius, the total loop concentration and the dislocation density as functions of irradiation time. It is interesting to note that the present model shows a reasonable agreement with experiment for the dislocation loop parameters. In comparing with experimental data, no correction was introduced for the resolution limit of the microscope. The average loop diameter in our comparisons are in the range of 10–100 nm, while the resolution limit is usually ~1 nm.

Finally, the effect of the irradiation temperature

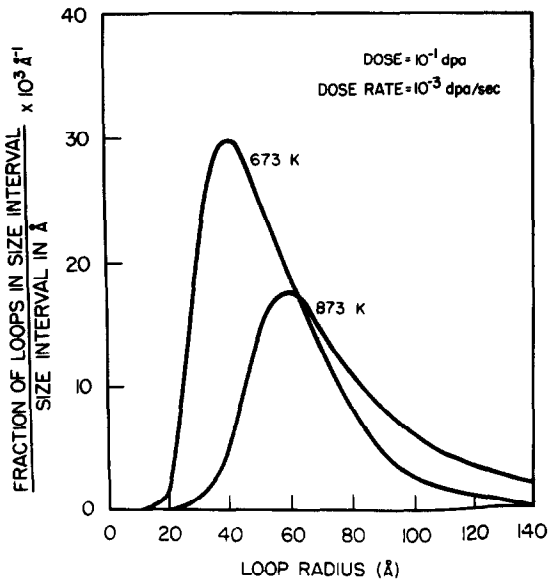

Fig. 13. Effect of irradiation temperature on the interstitial loop size distribution after a dose of 0.1 dpa.

on the interstitial loop distribution at 0.1 dpa is shown in fig. 13. A comparison between figs. 7 and 13 reveal that at the high dose rates, the peak height decreases considerably with increasing temperature. On the other hand, the temperature effect on the peak height is not as strong at the low dose rate. However, for both dose rates the higher temperature shifts the distribution towards larger values, which is consistent with the experimental findings.

7. Summary and conclusions

In this paper, we have developed a new method for calculating void and loop size distributions during irradiation. Small size interstitial clusters were studied using the detailed rate theory approach, while large-size loops were simulated by descretizing a transformed Fokker–Planck equation. This numerical approach allows the study of defects containing up to millions of atoms with very modest computational requirements. Microstructure parameters such as total defect concentrations, average size, defect distribution and moments, and total sink strength can be calculated as functions of irradiation time.

The results of the present hybrid approach have been compared to previous detailed rate theory computations. Various mesh sizes of the descretized Fokker–Planck equation resulted in interstitial loop size distributions that compare reasonably well with the rate theory calculations.

A simulation of low dose rate irradiations was carried out at 10^{-6} dpa/s, which is produced to within an order of magnitude in both fission reactor core components and fusion reactor first walls. It has been shown that the concentrations of small-size defect clusters reach equilibrium values after ~1000 s of irradiation. However, large size interstitial loops continued to develop with time lags that increased with increasing size. Interstitial loop fractioanl concentrations were found to be smaller by 1–2 orders of magnitude at 873 K when compared to 773 K. The total loop concentration and dislocation loop line density were found to decrease while the average size increased with increasing irradiation temperature, which is qualitatively consistent with fission reactor experiments.

A correlation with experimental data on heavy ion irradiated 316 stainless steel at 10^{-3} dpa/s was finally conducted. The numerical values obtained from the present model were shown to match reasonably well with the experimental data at 673 and 873 K. Total interstitial loop concentrations, average radii and total dislocation line densities were shown to be in reasonable agreement with the experimental data. Moreover, the qualitative behavior of the microstructure, which is probably more important than the absolute numerical values, showed the following trends:

(a) The loop concentration and dislocation density decrease with increasing temperature at the same dose and dose rate.

(b) For a fixed irradiation temperature and dose, the loop concentration and dislocation density increase rapidly with dose rate.

(c) The average loop size increases with increasing temperature at the same dose and dose rate, but decreases slightly with increasing dose rate if the total irradiation dose and temperature are constant.

(d) The growth speed of the interstitial loop distribution increases with increasing temperature.

The previous qualitative trends are consistent with the experimental data from fission reactors [25] and simulation facilities [26].

Acknowledgements

This work was supported by the National Science Foundation through Grant No. ENG78-05413.

References

[1] L.M. Brown, A. Kelly and R.M. Mayer, Phil. Mag. 19 (1969) 721.
[2] M. Kiritani, in: Proc. Conf. on Fundamental Aspects of Radiation Damage in Metals, Eds. M.T. Robinson and F.W. Young, CONF-751006-P2 (National Technical Information Service, US Dept. of Commerce, Springfield, VA, 1975) p. 775.
[3] M.R. Hayns, J. Nucl. Mater. 56 (1975) 267.
[4] N.Q. Lam, J. Nucl. Mater. 56 (1975) 125.
[5] R.A. Johnson, J. Nucl. Mater. 75 (1978) 77.
[6] B.O. Hall and D.I. Potter, in: Proc. 9th Intern. Symp. on Effects of Radiation on Structural Materials, Richland, WA, 1978.
[7] N.M. Ghoniem and D.D. Cho, Phys. Status Solidi (a) 54 (1979) 171.

[8] M. Kiritani, J. Phys. Soc. Japan 35 (1973) 95.
[9] M.R. Hayns, J. Nucl. Mater. 59 (1976) 175.
[10] M. Koiwa, J. Phys. Soc. Japan 37 (1974) 1532.
[11] M.R. Hayns, ref. [2], p. 764.
[12] J.A, Sprague, K.C. Russell and Y.H. Choi, ref. [2], p. 1181.
[13] W.G. Wolfer, L.K. Mansur and J.A. Sprague, in: Proc. Intern. Conf. on Radiation Effects in Breeder Reactor Structural Materials, Eds. M.L. Bleiberg and J.W. Bennet, Scottsdale, AZ, 1977, p. 841.
[14] B.O. Hall, J. Nucl. Mater. 91 (1980) 63.
[15] A.C. Damask and G. Dienes, Phys. Rev. 120 (1960) 99.
[16] N.M. Ghoniem and D.D. Cho, UCLA Engineering Report, UCLA-ENG-7845 (1978).
[17] S. Chandrasekhar, Rev. Mod. Phys. 15 (1943) 1.
[18] G.H. Weiss and M. Dishon, J. Statist. Phys. 13 (1975) 145.
[19] R.I. Cukier, K. Lakatos-Lindenberg and K.E. Shuler, J. Statist. Phys. 9, (1973) 137.
[20] D.R. Olander, Fundamental Aspects of Nuclear Reactor Fuel Elements (NTIS, 1976) p. 215.
[21] N.M. Ghoniem and G.L. Kulcinski, Radiation Effects 41 (1979) 81.
[22] R.A. Johnson, Phys. Rev. 152 (1966) 629.
[23] W.G. Wolfer and M. Ashkin, J. Appl. Phys. 46 (1975) 547.
[24] A.C. Hindmarch, LLL Report, UCID-3001, Rev. 3 (1974).
[25] H.R. Brager and J.L. Straalssund, J. Nucl. Mater. 46 (1973) 134.
[26] T.M. Williams, J. Nucl. Mater. 79 (1979) 28.
[27] N.M. Ghoniem and G.L. Kulcinski, Radiation Effects 39 (1978) 47.
[28] R.A. Johnson, J. Nucl. Mater. 83 (1979) 147.